

Information Processing Capability of Soft Continuum Arms

Estefany A. Torres¹, Kohei Nakajima^{2,3}, and Isuru S. Godage¹

Abstract—Soft Continuum arms, such as trunk and tentacle robots, can be considered as the “dual” of traditional rigid-bodied robots in terms of manipulability, degrees of freedom, and compliance. Introduced two decades ago, continuum arms have not yet realized their full potential, and largely remain as laboratory curiosities. The reasons for this lag rest upon their inherent physical features such as high compliance which contribute to their complex control problems that no research has yet managed to surmount. Recently, reservoir computing has been suggested as a way to employ the body dynamics as a computational resource toward implementing compliant body control. In this paper, as a first step, we investigate the information processing capability of soft continuum arms. We apply input signals of varying amplitude and bandwidth to a soft continuum arm and generate the dynamic response for a large number of trials. These data is aggregated and used to train the readout weights to implement a reservoir computing scheme. Results demonstrate that the information processing capability varies across input signal bandwidth and amplitude. These preliminary results demonstrate that soft continuum arms have optimal bandwidth and amplitude where one can implement reservoir computing.

I. INTRODUCTION

The advancement of bio-inspired soft continuum robots, featuring high compliance and inherent safety of operation in contrast to traditional rigid-bodied, precise but often dangerous robots, opens up novel research paradigms [1]–[3]. Continuum robotics is an umbrella term that herein is used to cover all types of active and physically reactive compliant systems. In this paper, we mainly focus on continuum robotic systems that can be bent, twisted and elongated, actively or passively, during operation. Continuum robots in this sense have often been made of elastomeric material or superelastic alloys, allowing them to change their shape with a few degrees of freedom (DoF) to form complex organic shapes (in contrast to fixed geometric shapes of rigid-bodied robots) and to be theoretically able to regulate stiffness over a broad range. Because of the passive deformation these robots undergo in the face of external forces, they can be considered as infinite DoF systems that are highly under-actuated. Continuum robotics has been a highly active area of research in the past few years. An impressive number of prototypes has been proposed over the years [4]–[7].

¹School of Computing, DePaul University, Chicago, IL 60604, USA. igodage@depaul.edu

²Graduate School of Information Science and Technology, The University of Tokyo, 7-3-1 Hongo, Bunkyo-ku, 113-8656 Tokyo, Japan

³JST, PRESTO, Kawaguchi, Saitama 332-0012, Japan k.nakajima@mech.t.u-tokyo.ac.jp

This work was supported in part by the National Science Foundation (NSF) grant number 1718755, and by JST PRESTO Grant Number JP-MJPR15E7, Japan, and JSPS KAKENHI Grant Numbers JP18H05472, JP16KT0019, and JP15K16076.

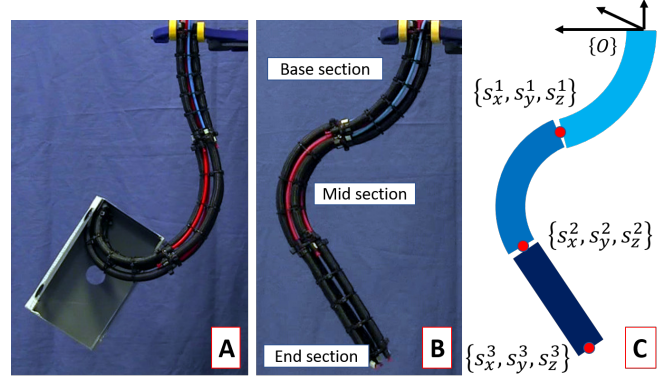


Fig. 1. (A) Pneumatically actuated multisection continuum arm designed at Italian Institute of Technology handling and object, (B) The same arm bending on a plane [9], and (C) Schematic of the prototype arm showing the coordinate convention and the output signal points (tip coordinates) used to record system response in this paper.

Yet control of continuum robots has not received as much attention, and therefore much of the control of continuum robots is limited to open loop control. Due to the presence of infinitely many DoF associated with inherent compliance, it became clear that controlling continuum robots are challenging. Kinematic control has been implemented on continuum robots wherein the robots are moved slowly in order not to invoke the compliance related oscillatory behaviors [8]. As a result, despite their enormous potential as human-friendly manipulators, continuum arms are primarily restricted to lab spaces, with their full potential remained to be realized.

Related to complex and compliant system control, a potentially ground breaking application is the study of morphological computations in which a robotic system uses its body dynamics (that are dependent on the configuration and physical properties such as stiffness and damping) to simplify control computations [10], [11]. In other words, some aspects of control can be outsourced to the body, using it as a computational resource, with the notion that these dynamic functions are already “encoded” within it. This approach can drastically reduce the complexity of the robot’s system dynamics computation and the corresponding control problems. A classic example of such embodied morphological intelligence related locomotion control is observed when the body of a dead fish starts swimming upstream when exposed to flowing water [12]. We can conclude that a fish can “outsource” the bulk of the neuromuscular coordination tasks to the “body”, without continuous oversight by the central nervous system, when the environmental conditions (hydrodynamic vortices) are right.

Recent works on morphological computational aspects for soft bodies [13]–[20] has shown that the mechanical properties of such infinite-dimensional bodies can be exploited as real-time computational assets. This approach is related to the reservoir computing framework [21]–[23]. The idea of a reservoir computing is to map inputs into a high-dimensional space so that the features of input signal can be linearly separable. This is achieved by training a learning system solely on readout signals and as a result it is ideally fit to understand the relationship of complex high dimensional physical systems such as soft continuum arms. Once a successful mapping is identified, the physical system itself can be used to compute and predict the behavior of the physical system, which could be used for controlling without the need of external controller, such as recurrent neural networks. The emulatability (or expression power) of such mapping is termed as the systems' information processing capability in this paper. Another key benefit of reservoir computing is that it is faster to train than traditional recurrent neural networks due to the simple learning schemes associated with it. In this paper, we will apply reservoir computing principles to investigate the information processing capability of the soft continuum arm shown in Fig. 1-A & B.

II. SYSTEM MODEL

A. Prototype Description

Each of the three continuum sections of the arm shown in Fig. 1-A are powered by three pneumatic muscle actuators (PMA). Each PMA is 0.15 m when unactuated and can extend up to 0.065 m at 600 kPa input pressure. A PMA is constructed from silicone rubber tube (inner diameter 7.5 mm and outer diameter 9.5 mm) as the PMA containment layer and polyester braided sheath (7 mm to 17 mm diameter range) as the outer layer to control the radial expansion and obtain extension. Nylon union tube connectors of inner diameter 4 mm are used to seal the Silicone tubes and facilitate air flow. More information about the fabrication of PMAs can be found in [24]. The PMAs of a single continuum section are mounted at 120° apart from each other and constrained in such a way that they maintain 0.0125 m length from the neutral axis (a hypothetical line that runs in the center of the arm cross-section). The 3D printed joints that connect adjacent continuum sections introduce a 60° angle offset about the neutral axis ($+Z$ axis of $\{O_i\}$). We use rigid plastic constrainers to maintain the PMAs in parallel to the neutral axis and provide improved torsional stiffness to minimize the possible deviations from constant-curvature deformation when operating under the influence of gravity. Each continuum section, inclusive of the tubing and constrainers has an approximate mass of 0.13 kg.

The pressure supply to the PMAs are precisely controlled by 9 digital proportional pressure regulators at 20 Hz that output pressures proportional to analog voltage signals between 0-10 V. The voltage signals are generated using a National Instrument PCI-6704 data acquisition card. The continuum arm motion in the workspace is tracked by using a Polhemus G4 wireless magnetic tracking system. The

tracking system allows high speed 6 DoF motion tracking at 100 Hz without subjected to occlusions (due to complex deformations) common in image-based tracking. In total, we mounted four trackers (two on the joints and one each on the origin and the tip of the end-section, see Fig. 1-C). The sensing and actuation are controlled by a Matlab Desktop Realtime Simulink model implemented on Matlab 2018a.

B. Dynamic Model

The information capacity search requires large number of data, typically involving more than 5000 randomly generated sample points at different amplitudes and fundamental signal frequencies (bandwidths). As reported in [24], [25] PMAs have a pressure deadzone, close to 100 kPa, where little to no extension is observed. The reason is that, in the pressure deadzone, the Silicon bladders undergo radial expansion within the braided mesh. Thus, the pressure range mapped to length changes is [100 kPa, 600 kPa] and we define 6 pressure amplitudes in that range (in 100 kPa intervals). Similarly, given the prototype arm's oscillatory behavior and the ability to respond quickly to fast input pressure signals, we define 7 time periods (1/8, 1/4, 1/2, 1, 2, 3, and 4) in which we will generate the systems responses. Further, for each combination of amplitude and time period, it is recommended to conduct number of trials to remove any bias from the input signals. Consequently, generating these results on the prototype robotic arm, particularly in the proof of concept stage, is not feasible. For instance, to generate 20 trials of 5,000 samples at fundamental period (bandwidth) 4 s, it will take 4×10^5 s. Therefore, the dynamic model developed for the prototype arm, detailed in [25], is used to generate the dynamic responses. The dynamic model was developed using the principles of integral Lagrangian formulation and runs at real-time efficiency. The model has been experimentally validated for step pressure responses, which included out-of-plane bending. In addition, the model, which was based on the constant-curvature assumption, maintained that assumption throughout those experiments. The model was implemented on Matlab Simulink 2018a. The input signals were then randomly generated, applied to the Simulink model, and the joint positions were calculated (joint-space variables are applied to the kinematic model [9]), and recorded. These data are then used in the processing stage, detailed in Sec. III-B.

III. METHODOLOGY

A. Dynamic Response Generation

The dynamic model of the prototype soft continuum arm shown in Fig. 1, as detailed in [25], is given by

$$\mathbf{M}\ddot{\mathbf{q}} + \mathbf{C}\dot{\mathbf{q}} + \mathbf{D}\dot{\mathbf{q}} + \mathbf{G} = \mathbf{F} \quad (1)$$

where $\mathbf{M} \in \mathbb{R}^{9 \times 9}$ is the generalized inertia matrix, $\mathbf{C} \in \mathbb{R}^{9 \times 9}$ is the centrifugal/Coriolis force matrix, $\mathbf{G} \in \mathbb{R}^9$ is the conservative force vector, and $\mathbf{F} \in \mathbb{R}^9$ is the input force vector. Physically, \mathbf{F} is the forces generated by the fluidic actuators.

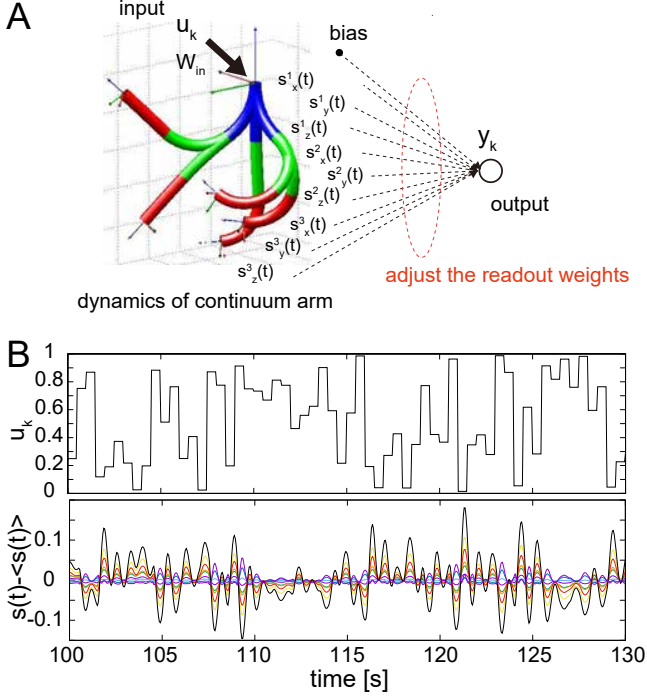


Fig. 2. Schematics showing the information processing scheme using the arm (A) and the typical body dynamics generated by the random motor commands (B). For (B), the upper plot shows the input series and the lower plot shows the corresponding normalized sensory time series. The parameter of the arm is set to $(A, \tau) = (2, 0.5)$.

We first generate a random input signal u with time steps of τ . Any $u(k)$ value of the input signal is kept constant until the next sample, $u(k+1)$.

Upon applying the input signal (pressures) to relevant PMAs, we measure the system response (i.e., motion) of the arm. We measure the position coordinates of each of the continuum section tips (see Fig. 1-C) and recorded at $\tau/10$ bandwidth. The choice for $10\times$ sampling rate (relative to the input signal bandwidth) ensures that the readout data is faithful to the actual motion of the arm in the range of τ we consider in this work. Otherwise, due to the fast dynamics of the prototype continuum arm (as documented in [25]), the recorded data will be incomplete and yields incorrect results. For instance, Fig. 2-B shows the plots of the input (top) and output coordinate (bottom) trajectories for $\tau = 0.5$. It can be seen that the smooth output data will be lost had the data were recorded at the input signal bandwidth $\tau = 0.5$ instead at $\tau = 0.05$.

B. Information Processing using the soft continuum arm

We here explain how to use our soft continuum arm as a reservoir. In this work, we only consider the base section of the continuum arm (see Fig. 1). The reason for this selection is two fold. First, it reduces the complexity of the input signal (3 in contrast to 9 signals). Second, because the sections are attached serially, base section has influence over the successive sections. As a result, we can observe how the physical excitation propagates along the length of arm via the compliant structure.

The input stream is injected to our system as addition of forces to the PMA actuators (also can be considered as active springs due to their high compliance) of the base section (the nearest to the base) with input weights $\mathbf{W}_{in} = [w_x \ w_y \ w_z]^T$. Throughout our analysis in this study, we use random real value in the range of $[0, 1]$ for the input u_k at timestep k . This is to avoid adding temporal correlations from the external signals, which is important when analyzing the information processing capability of figures/the arm itself. Furthermore, to see the effect of the amplitude of the input forces, input weights are assigned randomly from the range of $0 < w_x, w_y, w_z < A$, and the parameter A is controlled. This input is then transformed to a pressure signal by multiplying the amplitude of the pressure signal, A . The forces acting on the PMAs are then found by calculating the area over which the pressure is applied, $A\pi r^2$ where $r = 8\text{ mm}$ is the mean radius of PMAs during actuation. The corresponding outputs to this input stream are generated by the weighted sum of the joint coordinates (we call these, sensory values, $\{s_x^i, s_y^i, s_z^i\}$, for section i), which act as computational nodes in our setup (Fig. 2A). This implies that we have three sensory values for each section, and since we have three sections in this study, we have nine sensory values in total (Fig. 2B).

Here, we set parameter τ to regulate the timescale of each I/O computation (that is, a single timestep), in which a single computation takes the time range of τ [s] (Fig. 2B). Accordingly, we divide each time range τ into 10 fragments and correspond each sensory value (e.g., $\{s_x^1(k\tau + (\tau/10)), s_x^1(k\tau + 2 * (\tau/10)), \dots, s_x^1(k\tau + 10 * (\tau/10))\}$) to the input u_k . This implies that 10 values are fragmented for each sensory value, which samples $9 \times 10 = 90$ values in total. Using these sampled data, 90 computational nodes $\{x_k^1, x_k^2, \dots, x_k^i, \dots, x_k^{90}\}$ in total were prepared with reconfigured numbering i . Now, according to the inputs u_k provided to the system, the corresponding output y_k is calculated as $y_k = \sum_{i=0}^{90} w_{out}^i x_k^i$, where x_k^0 is set to 1 as a bias term and w_{out}^i is the readout weight of the i -th computational node.

In the reservoir computing framework, the learning of the target function \hat{y}_k is conducted by adjusting the linear readout weights w_{out}^i . During the training phase of the weights, the input stream is provided to the system, which then generates the arm motions, and the corresponding sensory time series is collected together with the target outputs for supervised learning. In this study, we apply a ridge regression, which is known as an L2 regularization, to obtain the optimal weights. In the evaluation phase, using the optimal readout weights, you drive the system with a new input stream and generate the system output, which is then used for the analysis of the performance. Throughout our experiments in this study, the washout phase, the training phase, and the evaluation phase are set to 500 timesteps, 2000 timesteps, and 2500 timesteps, respectively.

IV. RESULTS

In this section, the information processing capability of the soft continuum arm is investigated using numerical experiments. By using a benchmark task, which evaluates

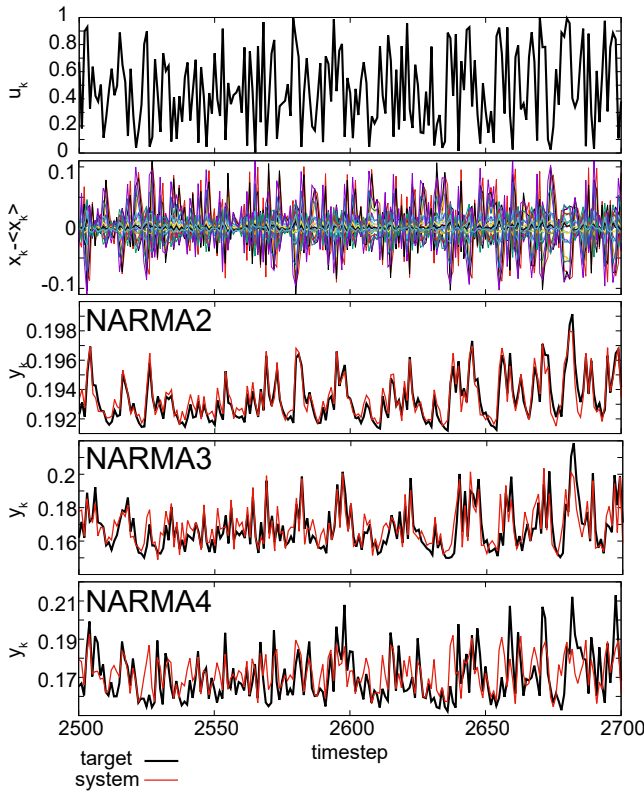


Fig. 3. Typical performances for NARMA tasks. Random input sequence (the upper line), the corresponding reservoir dynamics from 90 computational nodes prepared from the arm (the second upper line), and the corresponding target and system outputs are plotted for each NARMA task. The case for $(A, \tau) = (6, 1)$ is shown for example.

the capability to emulate nonlinear dynamical systems called *nonlinear auto-regressive moving average* (NARMA) system, and by assessing the linear and non-linear memory capacity, we demonstrate how the parameter (A, τ) affects the performance of our system systematically, where A is varied from 1 to 6 and τ is varied as 0.125, 0.25, 0.5, 1, 2, 3, and 4. The evaluation schemes adopted here are popular in the context of recurrent neural network learning.

A. Performance of NARMA tasks

The NARMA task is a benchmark task that is commonly used to evaluate the computational capability of the learning system to implement nonlinear processing with long time dependence. By calculating the deviations from the target trajectory in terms of errors, the NARMA task tests how well the target NARMA systems, which we introduce later, can be emulated by the learning system. According to the choice of the target NARMA system, we can investigate which type of information processing can be performed in the learning system. The first NARMA system that we examine is a second-order nonlinear dynamical system [26], expressed as follows:

$$y_k = 0.4y_{k-1} + 0.4y_{k-1}y_{k-2} + 0.6u_k^3 + 0.1, \quad (2)$$

and this system is called NARMA2 in this paper. The next NARMA system is the n th-order nonlinear dynamical

system, which is written as follows:

$$y_k = ay_{k-1} + a'y_{k-1}\left(\sum_{j=0}^{n-1} y_{k-j-1}\right) + a''u_{k-n+1}u_k + a''', \quad (3)$$

where $(a, a', a'', a''') = (0.3, 0.05, 1.5, 0.1)$. The order of the system n is varied from 3 to 9 in this experiment, and the corresponding systems are called NARMA n systems for simplicity. For the input stream to the NARMA systems, the range is linearly scaled from $[-1, 1]$ to $[0, 0.2]$ in order to set the range of y_k into the stable range. The performance is evaluated by comparing the system output with the target output in the evaluation phase using the *normalized mean squared error* (NMSE), expressed as follows: $NMSE = \frac{\sum_{k=2501}^{5000} (\hat{y}_k - y_k)^2}{\sum_{k=2501}^{5000} \hat{y}_k^2}$, where \hat{y}_k and y_k are the target output and the system output at timestep k , respectively. For each setting of (A, τ) , NMSEs for 20 trials, where the system is driven by a different random input sequence for each trial, are calculated and averaged for the analysis.

Figure 3 shows typical system outputs for the NARMA tasks in the evaluation phase, where the parameter is set to $(A, \tau) = (6, 1)$. We can see that, in particular for the NARMA2 emulation task, our system successfully traces the target NARMA system, and according to the increase of the order of the NARMA system, the overall task performance is gradually getting worse, suggesting the increase of the difficulty of the tasks. In Fig. 4, we have investigated the performance of the system in terms of NMSE systematically for each (A, τ) setting. We can clearly observe that, according to the order of the NARMA system, the tendency of the performance differs by the selection of the parameter (A, τ) . For example, for the NARMA3 task, the case for $\tau = 1$ showed the lowest NMSE, which suggests the highest performance, while other tasks showed the highest performance when $\tau = 0.125$. (The NARMA2 task also showed a good performance (although it was not the best) when $\tau = 1$.) These results imply that how to actuate the arm strongly affects the type of the information processing capability, which can be induced from the arm. We should note that one common tendency observed was that the parameter τ affected more dominantly than the amplitude of the input A to the task performance in this experimented parameter region.

B. Analysis of Linear and Nonlinear Capacities

Considering the fact that the information processing capability of reservoir dynamics can be characterized by its property of transforming the input stream, it has been proposed to express the system's information processing capacity by evaluating its emulatability of nonlinear functions over the input stream [27]. These functions are expressed as combinations of orthogonal functions, such as Legendre polynomials or Hermite polynomials, over each differently assigned delayed inputs. In this approach, the system's computational capability is decomposed into the degree of nonlinear processing and memory of the input that the system is capable to express. By exploiting the orthogonal functions,

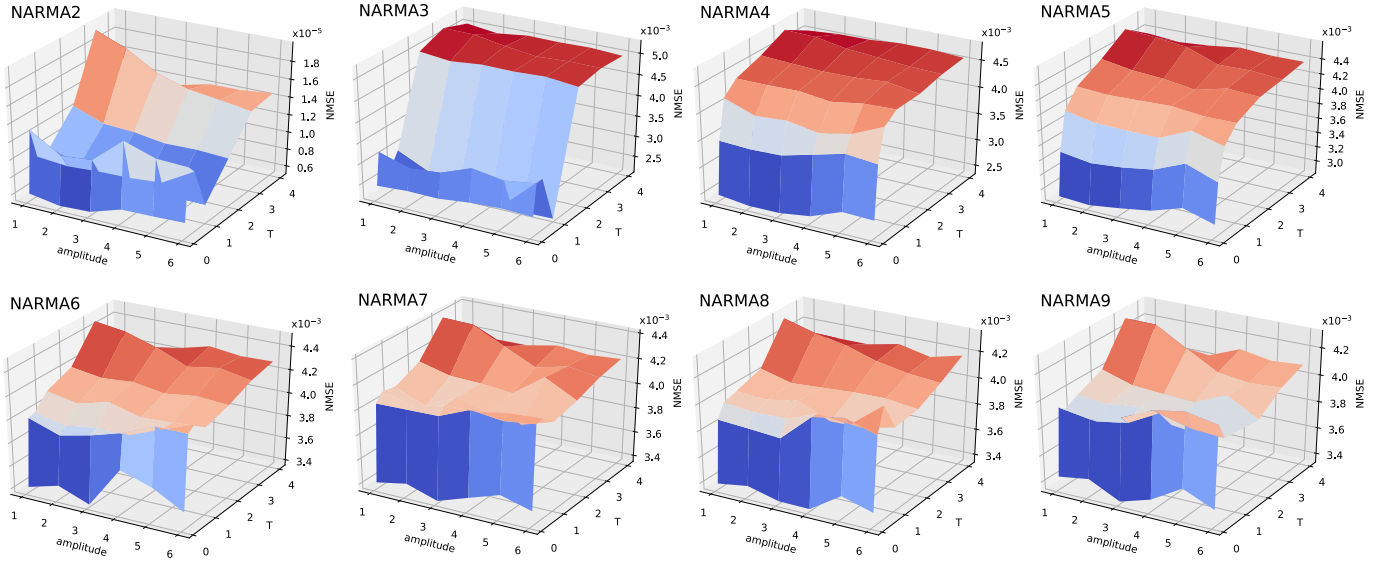


Fig. 4. Analyses of the performance of NARMA tasks in terms of NMSE according to each setting of (A, τ) .

the computational capability can be safely decomposed into several nonlinear functions without overlaps. In this paper, we do not investigate all the combinations of Legendre polynomials of the previous inputs, but exploit n -th order Legendre polynomials for each delay of input expressed as:

$$P_n(u_{k-d}) = 2^n \sum_{m=0}^n u_{k-d}^m \binom{n}{m} \left(\frac{n+m-1}{n} \right), \quad (4)$$

where $\binom{n}{m}$ is a binomial coefficient, and u_{k-d} is the input of d timesteps before from the timestep k . In this study, we varied the value of n from 1 to 10, and the delay d is varied from 0 to 50 and investigated how our system is capable of learning each polynomial systematically. Note that when $n = 1$, the polynomial becomes linear and it becomes equivalent to the case introduced in [28].

For the n -th order Legendre polynomials emulation task, using the system output time series, in each target function with given delay d , we calculate memory function of degree n , expressed as follows: $MF_d^n = \frac{\text{cov}^2(y_k, \hat{y}_k)}{\sigma^2(y_k)\sigma^2(\hat{y}_k)}$, where $\text{cov}(x, y)$ and $\sigma(x)$ express the covariance between x and y and the standard deviation of x , respectively. Then, the n -th order memory capacity C_n can be expressed as follows: $C_n = \sum_{d=0}^{50} MF_d^n$. By using the measure MF_d^n and C_n , we aim to evaluate the information processing capability of the our system. For each setting of n and d of the target Legendre polynomials, the learning scheme is exactly the same as explained previously, and, by using the 20 trials, the averaged MF_d^n and C_n are obtained for the analyses.

From the analyses of C_n , we first found that when n is larger than 6, the value approaches to zero in all of the investigated parameter region. This expresses the limitation of the expression power of the functions in our system. Figure 5 shows the results for $n = 1, 2$, and 3 for example. As we saw in the NARMA task, according to the degree of nonlinearity n of the target function, we can clearly observe that the

parameter region showing the highest capacity differs. For example, we can see the highest C_1 when $\tau = 0.125$, while the highest C_2 can be observed in $\tau = 0.5$ (Fig. 5). By increasing the degree of n higher than 3, we tend observe the highest value in the parameter region where τ is larger than 1 and the input amplitude A is larger than 4. Basically, as we saw in the case for NARMA task, the behavior of C_n was more dependent on the parameter τ than A , but for the degree of nonlinearity n larger than 3, the effect of the input amplitude A became dominant in the region of the high τ . Checking the MF_d^n profile, we can see that, in this region, the memory function when $d = 0$ is dominant, which means the immediate effect of input injection to the arm is exploited for the task performance (Fig. 5).

V. CONCLUSIONS

Due to high compliance, soft continuum arms have immense potential for applications in spaces with human presence. However, as a result of high compliance (passive DoF), control of such manipulators is still an open challenge. Learning-based approaches such as morphological computation and reservoir computing have shown promise to surmount this problem. In this paper, we investigated the information processing capability of a PMA powered soft continuum arm. We applied randomly generated input signals of 5000 sample points with varying amplitude and bandwidth to an experimentally validated dynamic model and recorded the system response. Using a benchmark task, which evaluates the capability to emulate nonlinear dynamical systems called *nonlinear auto-regressive moving average* (NARMA) system, and by assessing the linear and nonlinear memory capacity, we demonstrated how the parameter (A, τ) affects the performance of our system systematically. The results show that there are combinations of amplitude and bandwidth which operates the continuum arm in a domain most suited for reservoir computation based control implementation. In

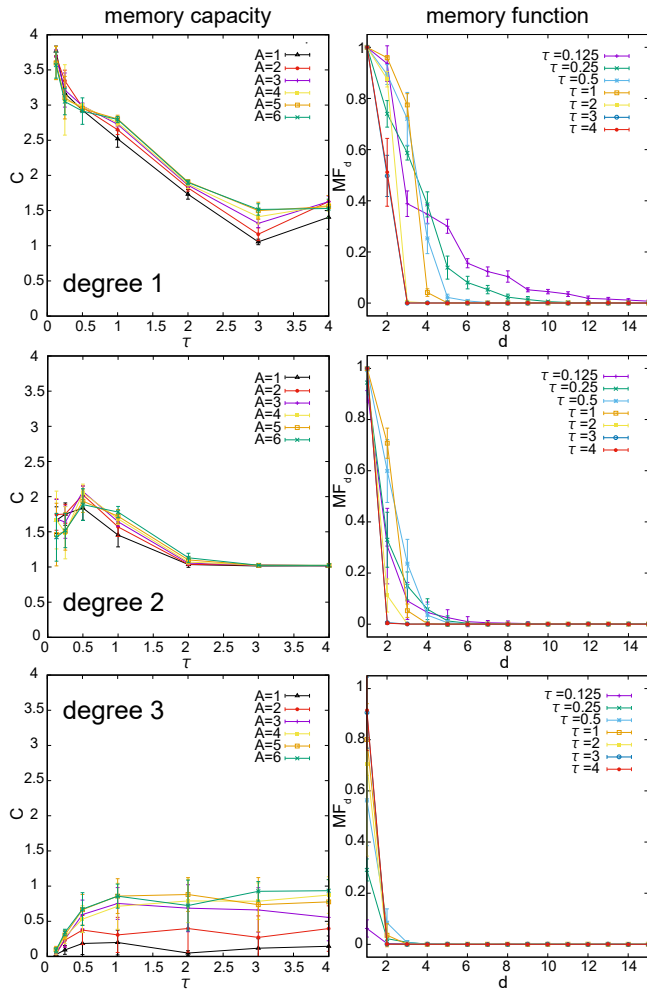


Fig. 5. Analyses of linear and nonlinear memory capacities and typical memory function for each parameter setting. Error bars show standard deviation.

future work, we will extend these qualitative results to validate the findings experimentally.

REFERENCES

- [1] D. Rus and M. T. Tolley, "Design, fabrication and control of soft robots," *Nature*, vol. 521, no. 7553, p. 467, 2015.
- [2] C. Laschi, B. Mazzolai, and M. Cianchetti, "Soft robotics: Technologies and systems pushing the boundaries of robot abilities," *Science Robotics*, vol. 1, no. 1, p. eaah3690, 2016.
- [3] G. Bao, H. Fang, L. Chen, Y. Wan, F. Xu, Q. Yang, and L. Zhang, "Soft robotics: academic insights and perspectives through bibliometric analysis," *Soft Robotics*, vol. 5, no. 3, pp. 229–241, 2018.
- [4] W. McMahan, V. Chitrakaran, M. Csencsits, D. Dawson, I. D. Walker, B. A. Jones, M. Pritts, D. Dienno, M. Grissom, and C. D. Rahn, "Field trials and testing of the octarm continuum manipulator," in *Robotics and Automation, 2006. ICRA 2006. Proceedings 2006 IEEE International Conference on*. IEEE, 2006, pp. 2336–2341.
- [5] A. Grzesiak, R. Becker, and A. Verl, "The bionic handling assistant: a success story of additive manufacturing," *Assembly Automation*, vol. 31, no. 4, pp. 329–333, 2011.
- [6] R. J. Webster III and B. A. Jones, "Design and kinematic modeling of constant curvature continuum robots: A review," *The International Journal of Robotics Research*, vol. 29, no. 13, pp. 1661–1683, 2010.
- [7] W. McMahan, B. A. Jones, I. D. Walker *et al.*, "Design and implementation of a multi-section continuum robot: Air-octor," in *IROS*, 2005, pp. 2578–2585.
- [8] T. Mahl, A. Hildebrandt, and O. Sawodny, "A variable curvature continuum kinematics for kinematic control of the bionic handling assistant," *IEEE transactions on robotics*, vol. 30, no. 4, pp. 935–949, 2014.
- [9] I. S. Godage, G. A. Medrano-Cerda, D. T. Branson, E. Guglielmino, and D. G. Caldwell, "Modal kinematics for multisection continuum arms," *Bioinspiration & biomimetics*, vol. 10, no. 3, p. 035002, 2015.
- [10] R. Pfeifer, F. Iida, and G. Gómez, "Morphological computation for adaptive behavior and cognition," in *International Congress Series*, vol. 1291. Elsevier, 2006, pp. 22–29.
- [11] H. Hauser, A. J. Ijspeert, R. M. Füchslin, R. Pfeifer, and W. Maass, "Towards a theoretical foundation for morphological computation with compliant bodies," *Biological Cybernetics*, vol. 105, no. 5-6, pp. 355–370, 2011.
- [12] D. Beal, F. Hover, M. Triantafyllou, J. Liao, and G. V. Lauder, "Passive propulsion in vortex wakes," *Journal of Fluid Mechanics*, vol. 549, pp. 385–402, 2006.
- [13] K. Nakajima, H. Hauser, R. Kang, E. Guglielmino, D. G. Caldwell, and R. Pfeifer, "Computing with a muscular-hydrostat system," in *Proceedings of 2013 IEEE International Conference on Robotics and Automation (ICRA)*, 2013, p. 14961503.
- [14] —, "A soft body as a reservoir: Case studies in a dynamic model of octopus-inspired soft robotic arm," *Frontiers in Computational Neuroscience*, vol. 7, p. 91, 2013.
- [15] Q. Zhao, K. Nakajima, H. Sumioka, H. Hauser, and R. Pfeifer, "Spine dynamics as a computational resource in spine-driven quadruped locomotion," in *Proceedings of 2013 IEEE/RSJ International Conference on Intelligent Robots and Systems (IROS)*, 2013, pp. 1445–1451.
- [16] K. Nakajima, T. Li, H. Hauser, and R. Pfeifer, "Exploiting short-term memory in soft body dynamics as a computational resource," *Journal of the Royal Society Interface*, vol. 11, no. 100, p. 20140437, 2014.
- [17] K. Caluwaerts, J. Despraz, A. İçen, A. P. Sabelhaus, J. Bruce, B. Schrauwen, and V. SunSpiral, "Design and control of compliant tensegrity robots through simulation and hardware validation," *J. Royal Society Interface*, vol. 11, no. 98, p. 20140520, 2014.
- [18] K. Nakajima, H. Hauser, T. Li, and R. Pfeifer, "Information processing via physical soft body," *Scientific Reports*, vol. 5, p. 10487, 2015.
- [19] —, "Exploiting the dynamics of soft materials for machine learning," *Soft Robotics*, vol. 5, no. 3, pp. 339–347, 2018.
- [20] K. Nakajima, T. Li, and N. Akashi, "Soft timer: dynamic clock embedded in soft body," in *Robotic Systems and Autonomous Platforms: Advances in Materials and Manufacturing*, S. M. Walsh and M. S. Strano, Eds. Woodhead Publishing in Materials, 2019, ch. 8, pp. 181–196.
- [21] W. Maass, T. Natschläger, and H. Markram, "Realtime computing without stable states: A new framework for neural computation based on perturbations," *Neural Computation*, vol. 14, no. 11, pp. 2531–2560, 2002.
- [22] H. Jaeger and H. Haas, "Harnessing nonlinearity: Predicting chaotic systems and saving energy in wireless communication," *Science*, vol. 304, no. 5667, pp. 78–80, 2004.
- [23] D. Verstraeten, B. Schrauwen, M. dHaene, and D. Stroobandt, "An experimental unification of reservoir computing methods," *Neural Networks*, vol. 20, no. 3, pp. 391–403, 2007.
- [24] I. S. Godage, D. T. Branson, E. Guglielmino, and D. G. Caldwell, "Pneumatic muscle actuated continuum arms: Modelling and experimental assessment," in *Robotics and Automation (ICRA), 2012 IEEE International Conference on*. IEEE, 2012, pp. 4980–4985.
- [25] I. S. Godage, G. A. Medrano-Cerda, D. T. Branson, E. Guglielmino, and D. G. Caldwell, "Dynamics for variable length multisection continuum arms," *The International Journal of Robotics Research*, vol. 35, no. 6, pp. 695–722, 2016.
- [26] A. F. Atiya and A. G. Parlos, "New results on recurrent network training: Unifying the algorithms and accelerating convergence," *IEEE Trans. Neural Netw.*, vol. 11, p. 697, 2000.
- [27] J. Dambre, D. Verstraeten, B. Schrauwen, and S. Massar, "Information processing capacity of dynamical systems," *Scientific reports*, vol. 2, p. 514, 2012.
- [28] H. Jaeger, "Short term memory in echo state networks," *GMD-Forschungszentrum Informationstechnik*, vol. 5, 2001.